Right-Moving Supercell Tornadogenesis during Interaction with a Left-Moving Supercell's Rear-Flank Outflow

ROGER EDWARDS[a] AND RICHARD L. THOMPSON[a]

[a] *NWS Storm Prediction Center, Norman, Oklahoma*

(Manuscript received 16 May 2023, in final form 8 November 2023, accepted 16 November 2023)

ABSTRACT: On the local afternoon of 29 May 2012, a long-lived, right-moving (RM) supercell formed over northwestern Oklahoma and turned roughly southeastward. For >3 h, as it moved toward the Oklahoma City, Oklahoma, metro area, this supercell remained nontornadic and visually high-based, producing a nearly tornadic gustnado and a swath of significantly severe, sometimes giant hail up to 5 in. (12.7 cm) in diameter. Meanwhile, a left-moving (LM) supercell formed over southwestern Oklahoma about 100 mi (161 km) south-southwest of the RM storm, and moved northeastward, with a rear-flank gust front that became well defined on radar imagery as the LM storm approached southern and central parts of the metro. The authors, who had been observing the RM supercell in the field since genesis, surmised its potential future interaction with the LM storm's trailing gust front about 1 h beforehand. We repositioned to near the gust front's extrapolated collision point with the RM mesocyclone, in anticipation of maximized tornado potential, then witnessed a small tornado from the RM mesocyclone immediately following its interception of the boundary. Synchronized radar and photographic images of this remarkable sequence are presented and discussed in context of more recent findings on tornadic supercell–boundary interactions, with implications for operational utility.

SIGNIFICANCE STATEMENT: Supercells—well-organized, rotating thunderstorms mainly found in midlatitudes—commonly produce the largest hail, along with damaging gusts and most tornadoes. In radar imagery and photographs, we show the characteristics and merger of two supercell types: left-moving and right-moving, with respect to winds aloft. As the left-moving storm's trailing gust front interacted with the right-mover's mesocyclone, the latter strengthened quickly, soon producing a tornado. Observed evolution of these storms supports idealized numerical and conceptual models for supercell behavior and interactions with storm-scale boundaries, and may be useful in short-fused tornado forecast and warning operations.

KEYWORDS: Gust fronts; Severe storms; Supercells; Tornadoes; Convective storms; Operational forecasting

1. Background and meteorological overview

Supercell thunderstorms in the United States offer the full spectrum of convective severe weather, including around 99% of all reports of giant hail (diameter ≥ 4 in. or 102 mm; Blair et al. 2011), as well as severe gusts, a majority of tornadoes and nearly all violent tornadoes (Smith et al. 2012; Thompson et al. 2012). Analysis and short-fused forecasting of supercells and their impacts is complicated operationally by the many types of storm and boundary mergers that have been observed and simulated (e.g., Lindsey and Bunkers 2005; Hastings and Richardson 2016; Fischer and Dahl 2023), but that remain an enigma in severe storms prediction. In this work, we use radar and photographic imagery and mesonet data to document and analyze one specific boundary–supercell interaction type, where its tornado potential was anticipated correctly in the field, and also can be in operations: a mesocyclone's ingestion of the gust front from an anticyclonic supercell.

During the local afternoon and evening of 29 May 2012 (29–30 May in UTC), several supercells developed east of a dryline and south of a warm front across southern and eastern Kansas, western and central Oklahoma, and north Texas. In the SPC severe thunderstorm reports database—accessible via https://www.spc.noaa.gov/wcm/#data and documented by Schaefer and Edwards (1999)—these thunderstorms produced the bulk of 118 severe hail reports, 48 severe or damaging convective wind events, and 2 small tornadoes across the same areas, through 1200 UTC 30 May 2012. This case study documents two of the supercells—one right-moving (RM), one left-moving (LM), which initiated about 100 mi (161 km) apart, and later interacted as the RM storm produced one of those tornadoes. Given the importance of observed storm–storm and storm–boundary interactions in regulating tornado potential (e.g., Markowski et al. 1998; Lee et al. 2006; Tanamachi et al. 2015), this case represents one type of favorable interaction.

Typical of late spring, the southern fringe of the stronger winds aloft extended from the southern Rockies to the southern Great Plains, between ridging over Mexico and a trough over the upper Great Lakes (not shown). West-northwesterly midtropospheric flow transported steep midlevel lapse rates eastward over the southern and central Great Plains from the Rockies, atop low-level moisture spreading northward across Texas and Oklahoma. The 0000 UTC 30 May 2012 observed sounding at Norman, Oklahoma, characterized the potential for

Supplemental information related to this paper is available at the Journals Online website: https://doi.org/10.1175/WAF-D-23-0075.s1.

Corresponding author: Roger Edwards, roger.edwards@noaa.gov

DOI: 10.1175/WAF-D-23-0075.1

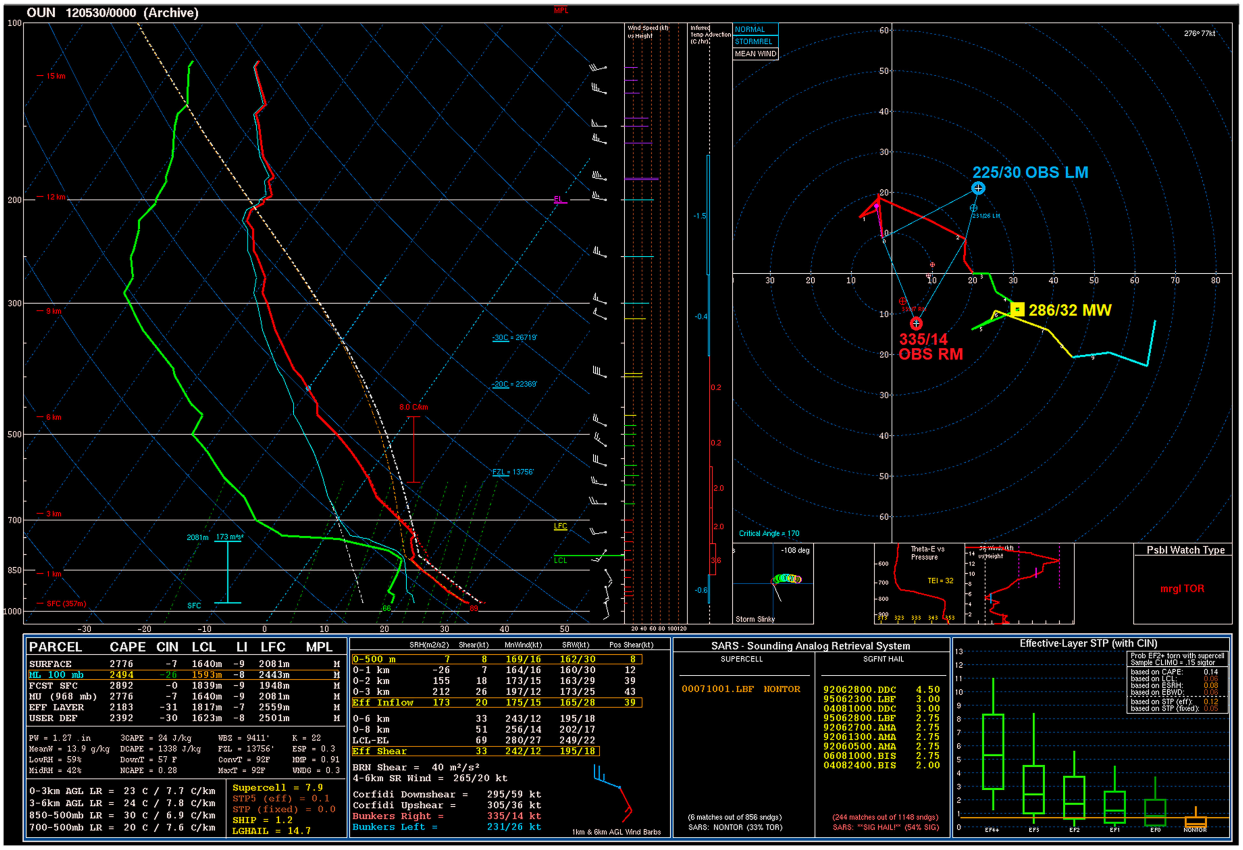

FIG. 1. Sounding for Norman, OK (OUN), 0000 UTC 30 May 2012, represented by (left) skew T–log$p$ and (right) hodograph, with common SPC-NSHARP-derived parameters below, similar to the Python-based successor SHARPpy (Blumberg et al. 2017). Observed RM (thick red circle and label) and LM (thick blue circle and label) motions are added to the hodograph, with mean wind highlighted in yellow. Bunkers et al. (2000, 2014) RM and LM motions are represented by nearby, labeled, filled red and blue markers, respectively. Kinematic-related parameters are valid for the RM storm.

both left- and right-moving supercells with large buoyancy, weak convective inhibition, and a relatively long, straight hodograph (Fig. 1). This sounding was within the 40–80-km and 1–2-h ranges recommended by Potvin et al. (2010) for supercell proximity soundings.

2. Evolution and interaction of supercells

The supercells initiated in northwestern (RM) and southwestern (LM) Oklahoma, and interacted over western portions of the Oklahoma City, Oklahoma, metro area. Figure 2 shows geographic locations of counties, municipalities, radar sites, and Oklahoma Mesonet (Brock et al. 1995) stations mentioned throughout the text, as well as approximate tracks of the RM and LM supercells' reflectivity centroids, and distance scale for spatial reference. Convective modes described herein are classified based on the methods of Smith et al. (2012). Each supercell was discrete through maturity before their merger, with the tornadic storm being a cyclonically rotating RM supercell, and the influential boundary producer being an anticyclonic LM. As such, they can be represented in an idealized, two-dimensional schematic, patterned after that of Lemon and Doswell (1979, hereafter LD79) for the RM, and its mirrored LM after Figs. 1g and 1h of Edwards and Hodanish (2006).[1] We adapted their schematics here as Fig. 2, as follows: reshaped the supercell outlines, their outflow boundaries and relative positions to approximate the precollision radar imagery shown below, and added annotations for the sign of the surface-flow curvature and associated vorticity accompanying the trailing gust fronts.

a. *Pretornadic RM supercell*

The RM supercell we observed also was a target of intensive scientific field study. Aircraft and ground crews with the Deep Convective Clouds and Chemistry (DC3) field program (Barth et al. 2015) sampled the environment in and around

[1] Since LD79, numerous observational and modeling studies (e.g., Beck and Weiss 2013) have described and illustrated supercells with much more complex four-dimensional structures than portrayed by the idealized LD79 schematic. Beatty et al. (2008) offer an overview of the evolution of supercell precipitation distribution via several schematics. Still, since our case fundamentally conformed well to it, we use the widely recognizable LD79 archetype and its LM version for comparison herein.

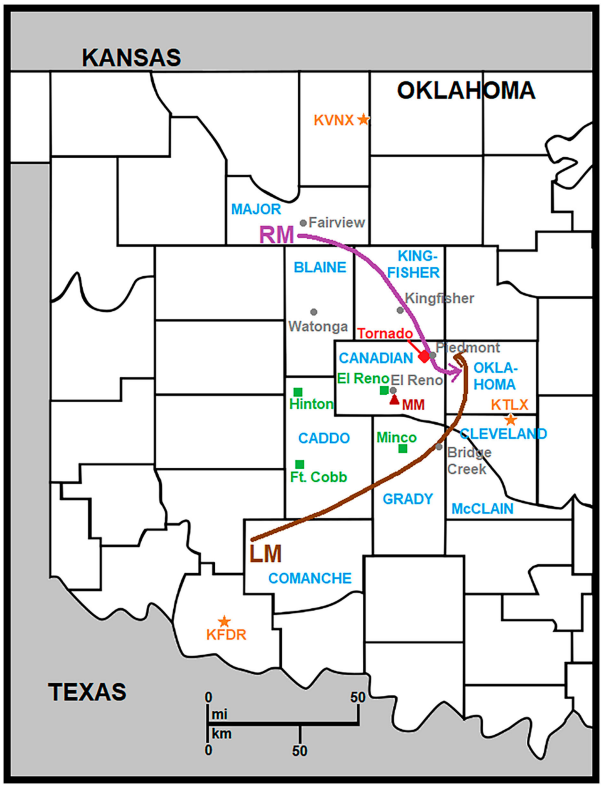

FIG. 2. County map of western and central Oklahoma, labeled as follows: states (black), affected counties (blue), cities and towns in text (gray filled circles), Oklahoma Mesonet sites (green squares), RM path (purple), and LM path (brown). Radar sites (orange stars): Twin Lakes (KTLX), Vance Air Force Base (KVNX), and Frederick (KFDR). The 0054 UTC DC3 MM location is marked by a dark red triangle. The tornado is located at the red diamond.

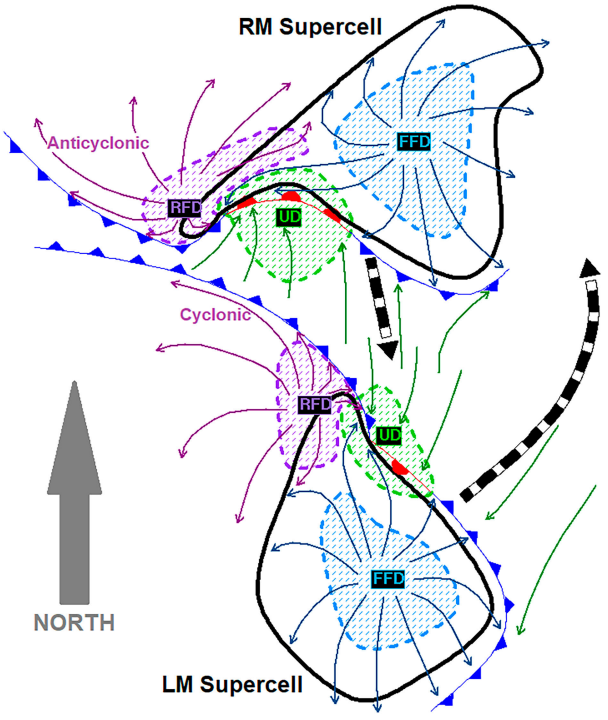

FIG. 3. Idealized LD79-type schematic of the RM supercell, and for the LM storm, similarly to Edwards and Hodanish (2006). Gust fronts labeled using conventional frontal symbology. Both supercells' shapes and relative positions are adapted to those herein at ≈0110 UTC 29 May 2012. FFD stands for forward-flank downdraft, RFD for rear-flank downdraft, UD for updraft. *Storm-relative* surface flow is depicted by streamlines, with sign labeled in purple for areas behind the trailing part of each gust front. Inflow is green; outflow is blue (FFD) and purple (RFD). Thick black arrows represent supercell motion over the ensuing ≈15 min.

the storm during its long pretornadic phase. This included balloon-borne, in situ observations and documentation of precipitation particles and microphysics in the supercell from an instrument launched at 2323 UTC (Waugh et al. 2015). For more-detailed DC3 observations and discussion of the pretornadic RM supercell's near-storm environment, especially during its rapid intensification stage prior to reaching Kingfisher (Fig. 3), see Davenport et al. (2019). They examine two key aspects: 1) the maturing and newly matured supercell's observed inflow environment, and 2) numerically simulating this storm, while modulating a typically homogeneous modeled storm environment via DC3 data. Though not formally participating in the project, we observed real-time project data and shared our forecast insights with a familiar DC3 ground crew in Watonga, Oklahoma, before convection leading to the supercell initiated about 25 mi (40 km) to our north-northwest.

The first 35-dBZ echo associated with what would become the RM supercell was evident at 2150 UTC from the nearest WSR-88D unit at Vance Air Force Base, Oklahoma (KVNX, not shown). The echo appeared east of a dryline, over the western part of the Blaine/Major County line, around 4–8 mi (6.4–12.8 km) south of Fairview, Oklahoma. We observed the growing convection visually from south-southeasterly to east-southeasterly perspectives. The associated towering cumuli and cumulonimbus developed into the southern part of an anvil canopy from a young thunderstorm over Fairview. Though they remained distinct visually, 5.1° beam-elevation reflectivity indicated the 35-dBZ echoes briefly connected on their eastern (downshear) underanvil periphery, at 2159 UTC, before separating permanently. The northern echo dissipated, with the southern cell's associated towers visually "taking over" as the main updraft area, and providing further cloud mass to their common anvil canopy. The resulting thunderstorm moved eastward roughly parallel to the same county line until about 2234 UTC. The thunderstorm then turned southeastward, while developing cyclonic quasi-horizontal (along-beam) shear and exhibiting broad, 35-kt (18 m s^{-1}) rotational velocity (V_{rot}) around 4.0° beam tilt, or 17 000 ft (5182 m) above radar level (ARL) in the midlevels.

Cyclonic rotation deepened but remained broad in the resulting supercell, which developed a well-defined, high updraft base visually as it moved southeastward into northwestern Kingfisher County. Reports of severe (≥1 in. or 2.5 cm) hail had begun beneath this storm's forward-flank core. Accordingly, we maintained

a generally southerly to southeasterly position with respect to the updraft through 2306 UTC, the time of the reflectivity, base velocity and photograph shown in Fig. 4. From this point onward, radar imagery is from the "Twin Lakes" (KTLX) WSR-88D near Oklahoma City, to offer a common comparative frame of reference with single-site radar vantage, for the remainder of the evolution of both this RM supercell and the LM storm discussed in the next subsection.

At 0008 UTC, with the forward-flank core of the RM supercell over central Kingfisher County, north of the city of Kingfisher (Fig. 5), it remained high-based. A visually well-developed rear-flank downdraft (RFD) lofted and advected dust southward and southeastward around the west side of the low-level mesocyclone and an associated wall cloud. Within the RFD outflow-dust plume, southwest of the wall cloud, a cyclonic gustnado (Doswell 1985) developed, at first entirely disconnected from the updraft. Its upper portion then bent toward and appeared to entrain into the *subcloud* updraft region before the entire feature lost definition. As this vortex never made verifiable visual contact with the cloud base and deeper convective column during its ≈1-min life-span, we neither categorized nor reported it as a bona fide tornado. We also cannot rule out brief contact between an unseen higher part of the vortex and the deep convective cloud.

At the location of Fig. 5, we examined available radar imagery from KTLX, noticing the approaching LM storm and its own readily apparent RFD gust front (section 2b). Surmising its potential cyclonic-vorticity augmentation upon interacting with the RM mesocyclone, we repositioned toward the extrapolated merger of the RM mesocyclone and LM gust front near Piedmont, Oklahoma. Meanwhile, SPC hail data indicate that the portion of the RM supercell's forward-flank core near the mesocyclone produced up to 4.5-in. (11.4-cm)-diameter hail at Kingfisher from 0038 to 0054 UTC. The supercell then moved south-southeastward into Canadian County with a manually determined vector from 335° at 14 kt (7.2 m s^{-1}), similar in direction but twice the speed prescribed by Bunkers et al. (2000), from the proximity sounding of Fig. 1. Reports of 4–5-in. (10.2–12.7-cm)-diameter hail—the largest from this storm—occurred at Piedmont from 0115 to 0125 UTC, just before and during the tornado discussed in section 2c.

b. *LM supercell before RM interaction*

The LM supercell developed in northwestern Comanche County at about 2227 UTC, based on the first associated 35-dB*Z* echo from the nearest WSR-88D at Frederick, Oklahoma (KFDR), appearing in a column through 7.6°, 8.8° and 10.1° beam tilts (not shown). Those beam heights, at that range, sample a middle–upper-tropospheric layer from 18 100 to 24 800 ft (5517–7559 m) above the KFDR radar level. Storm genesis was ≈100 mi (161 km) south-southwest of the maturing RM storm, which was astride the eastern Major/Blaine County line at the time, prior to Fig. 4. The LM thunderstorm formed not from a split, but instead, as an outflow boundary from a preexisting, disorganized, multicell thunderstorm to its west moved east-northeastward, intercepting the uplift side of one in a series of southeast–northwest-oriented horizontal convective rolls (HCRs; Wilson et al. 1994; Weckwerth et al. 1997), evident from KFDR (not shown). Similar HCRs were evident as wavy, low-reflectivity features from KTLX, where the lowest beam elevation did not overshoot them (Fig. 4 and the supplemental animation, east of the newly formed LM). Moist-sector supercell genesis involving HCRs has been documented, including the historically destructive, tornadic "Storm A" on 3 May 1999, which initiated within one county south of this LM genesis location (Edwards et al. 2000; Thompson and Edwards 2000).

In step with the motion of the associated outflow boundary, the LM echo proceeded east-northeastward and intensified, as evident in abrupt (one volume scan) increases and expansions in columnar reflectivity upon encountering each succeeding HCR's uplift side for at least another 1 h. Meanwhile, the initial thunderstorm associated with the outflow boundary closely followed the newer LM storm across northern Comanche County, then dissipated by 2330 UTC, as the LM storm obliquely entered southern Caddo County. The LM storm's net motion vector then backed slightly to northeastward (more leftward deviation) as it matured, with anticyclonic along-beam shear becoming evident in KTLX base-velocity imagery, as the storm enlarged and intensified across Caddo and Grady Counties. Snapshots of the LM storm's life-span from KTLX also are annotated in Figs. 4 and 5 (and later in Fig. 7), with the RM discussed in section 2a above. As the LM supercell crossed northeastern Grady and extreme northwestern parts of McClain and Cleveland Counties, approaching Oklahoma County and its impact on the RM supercell, the LM storm moved northeastward (from 225° at 30 kt or 15.4 m s^{-1}). This motion was similar in direction and about 87% the speed of the Bunkers et al. (2000) LM vector (Fig. 1), and more than twice the speed of the RM storm. During this close-approach stage, the LM supercell's forward-flank core also produced its largest hail report: 2.75 in. (7 cm) in diameter over extreme northwestern McClain County.

Different parts of the premerger LM gust front passed across four then-operating Oklahoma Mesonet sites (map in Fig. 3), in chronological order (Table 1): Ft. Cobb, Minco, Hinton, and El Reno, Oklahoma. (The current, ideally positioned Yukon mesonet did not exist in 2012.) Each site recorded perturbations in temperature, dewpoint, wind speed, and wind direction during, or within 10 min of, the boundary's overhead passage in radar reflectivity and/or velocity. Being the closest sites along the gust front to the LM supercell, Minco and El Reno exhibited the greatest effects (Fig. 6). Pressure rises immediately after the boundary, followed by falls, were well-defined and followed the conceptual model of traveling across the storm-scale pressure high or ridge inherent to the trailing cold pool. The closest station to the LM rear flank was Minco (Fig. 6, right side), where on radar, gust-front passage was followed almost immediately (within the 5-min data resolution) by the hook echo, then the post-supercellular outflow air. The gust front expectedly lowered temperature and dewpoint (Figs. 6c,d), conterminous with wind shifts and speed and gust increases (Figs. 6d–h). Consistent with immediate approach and passage of the LM mesocyclone nearly overhead at Minco, winds veered sharply, then backed for 30 min from the rear side of the mesocyclone into the trailing cold pool (an analogous RM mesocyclone sequence would entail backing, followed by veering behind the mesocyclone and rear-flank gust front).

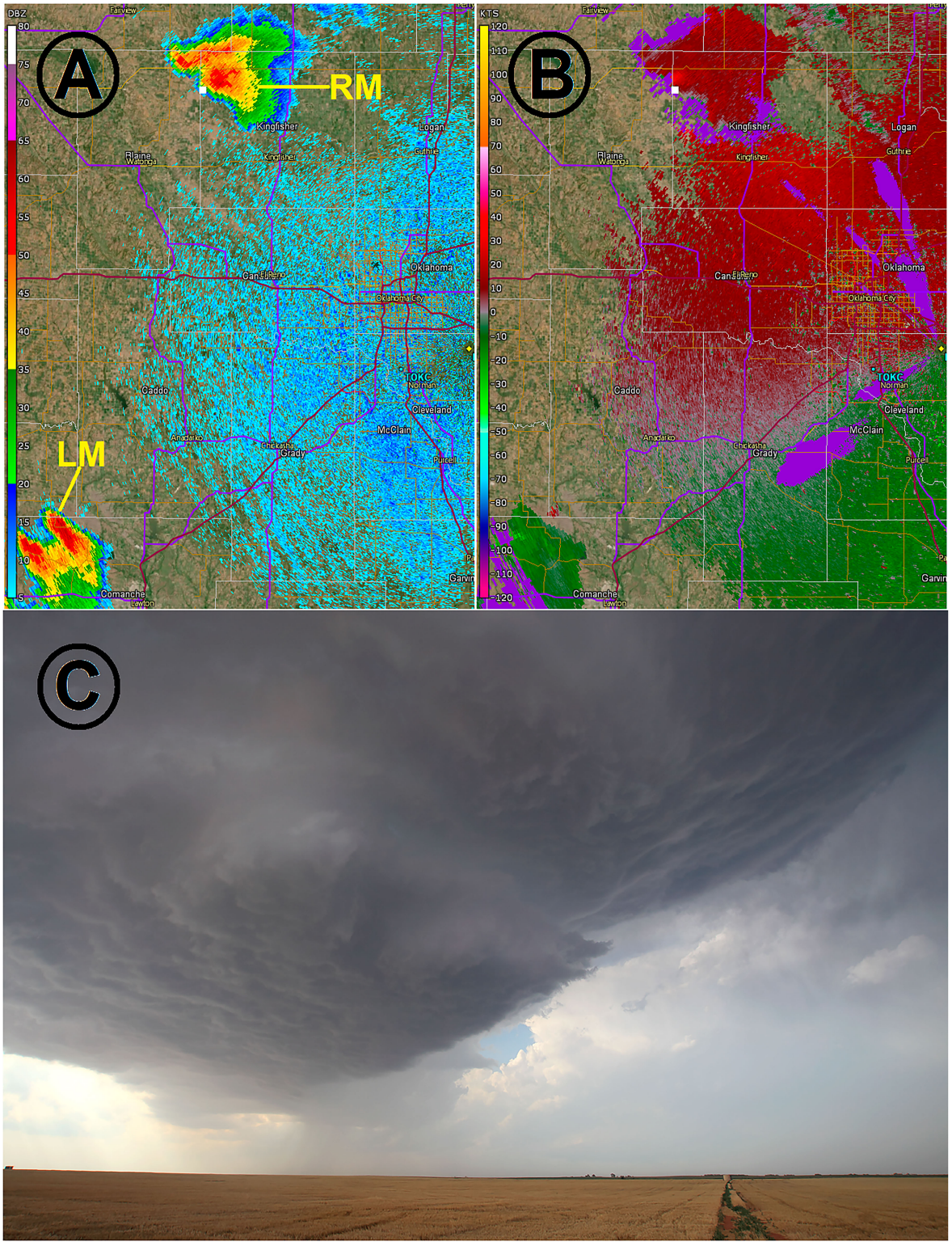

FIG. 4. All images at 2306 UTC 29 May 2012, with panels from the KTLX radar shown at 0.5° beam elevation: (a) base reflectivity, (b) base velocity matching the spatial coverage of (a),(c) full-frame digital photograph looking north-northwest at 19-mm wide-angle focal length, showing a high-based wall cloud (which was rotating only weakly) from GPS location 36.058°, −98.1974°. (If pasting into mapping engine, use a hyphen for the negative value.) The yellow dot at the far right on the radar imagery denotes the radar location. The white square denotes the photo position next to the RM storm, with RM and LM storms labeled in (a). Radar display courtesy GRLevel2. (Photo by lead author R. Edwards.)

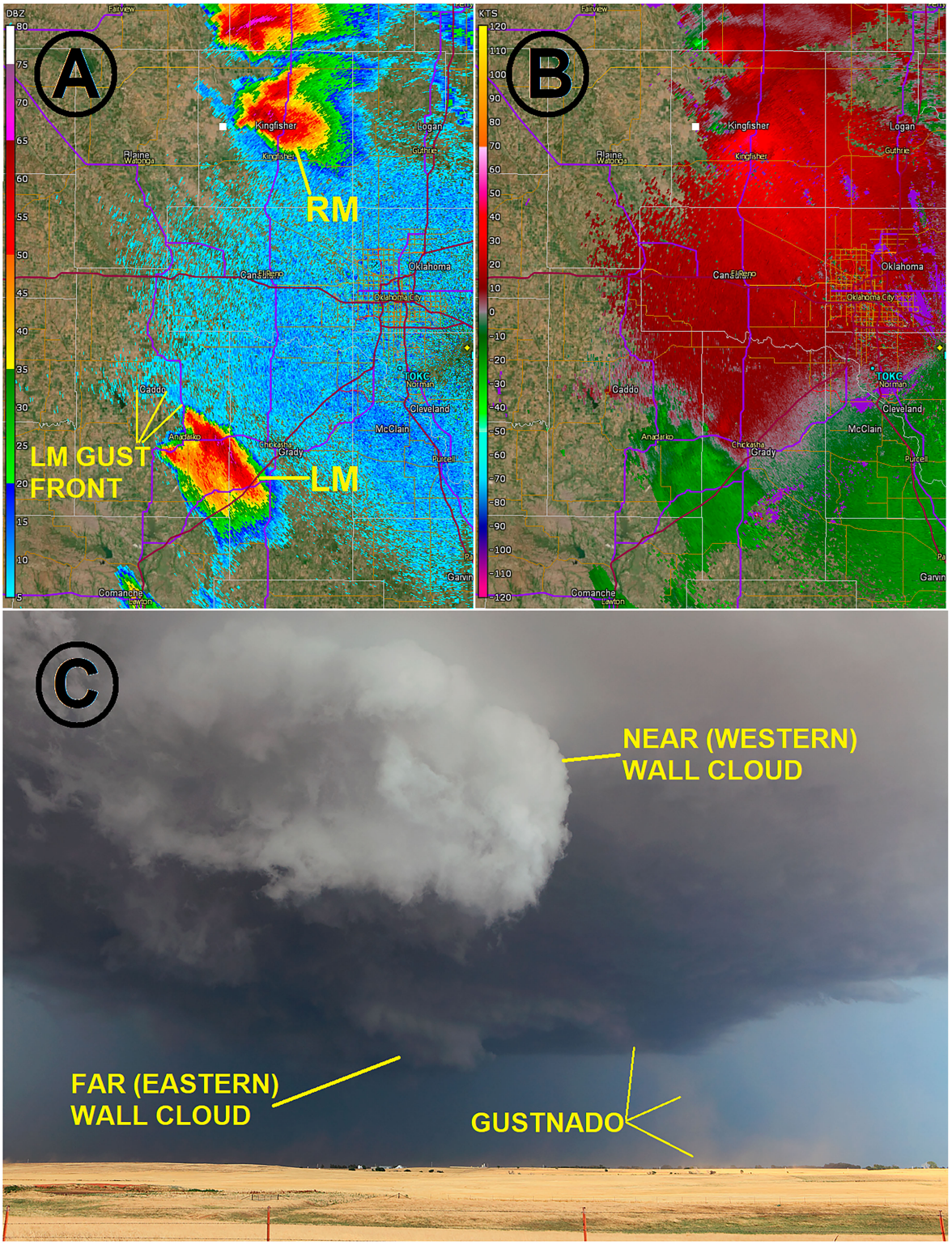

FIG. 5. (a)–(c) As in Fig. 4, but for 0008 UTC 30 May 2012, with LM gust front labeled. Diffluent outbound (easterly) velocity component is evident in the LM gust front in (b). Photo position was 35.9512°, −98.1211°, looking east, with 34-mm focal length. Gustnado is labeled on the photo to the lower right (south) of the nearest (western) RM wall cloud. Another wall cloud (also labeled) is evident in the distance.

TABLE 1. Mesonet station specifications (courtesy Oklahoma Mesonet) with KTLX 0.5° beam-center height above radar level (from GRLevel2), and approximate time of LM gust-front passage relative to 5-min interval of mesonet data. MSL height of radar is 1214 ft (371 m). ARL is above radar level.

Site name	Location (lat, lon)	MSL site elevation [ft (m)]	KTLX 0.5° ARL beam elevation [ft (m)]	LM gust-front passage (UTC)
Fort Cobb	35.1489°, −98.4661°	1375 (419)	5384 (1641)	2350
Minco	35.2723°, −97.9555°	1617 (493)	2468 (752)	0035
Hinton	35.4844°, −98.4815°	1411 (430)	5397 (1645)	0040
El Reno	35.5485°, −98.0365°	1384 (422)	3058 (932)	0100

Though DC3 operations officially had stopped, an affiliated mobile mesonet (MM) still was gathering data, when the LM gust front passed overhead, 5 mi (8 km) south-southeast of El Reno at 0054 UTC (position in Fig. 3). This was about 6 min before the boundary reached the El Reno fixed mesonet site. Based on GPS logs accompanying the data, the vehicle had pulled off U.S.-81 on a gravel side road, restarted eastward, was slowing down to turn back southward on U.S.-81 when the gust front passed overhead. Then in outflow air, the MM turned south and accelerated to normal highway speeds (≈30 m s^{-1}) after entering U.S.-81 again. Pressure, thermodynamic, and wind data (natively corrected for vehicle motion) were sampled at ≈1-s intervals, then smoothed to 1-min intervals for analysis in the same 110-min bracket as Fig. 6. Similar trends were noted in temperature, dewpoint, and wind behavior (not shown) as at the El Reno fixed site, while the MM penetrated the gust front and quickly passed deeper into its outflow air. Direct comparisons of the fixed versus MM data (especially absolute pressure) are problematic, though, because of differences between the platforms regarding sampling interval, instrument height AGL, perturbations by passing vehicles, nonlinear variations on pressure imparted simultaneously by changes in both MM altitude and thermal properties of ambient air, and the unevenly accelerated timeline of a variably moving versus fixed platform's passage through the same features.

c. *RM–boundary interaction, tornado, and aftereffects*

Within ≈15 min before the LM gust front reached the RM supercell, we had relocated to near Piedmont, along Oklahoma Highway 3, ahead of and between both features. Meanwhile, unknown to us, an SPC mesoscale discussion (https://www.spc.noaa.gov/products/md/2012/md0971.html) (see Edwards et al. 2015 for general product description) was being formulated, noting the same features, while specifically mentioning the incipient boundary–supercell interaction and related heightened short-fused tornado potential in Canadian and Oklahoma Counties (transmitted at 0121 UTC). The boundary noticeably passed our location at 0115 UTC, evident via wind shift and surface cooling. Within <5 min thereafter, the cloud base lowered and its rotation strengthened markedly, as the boundary at lowest radar-beam elevation (0.5°, ≈2800 ft or 850 m ARL) passed the RM supercell's reflectivity hook. The tornado began at 0121 UTC (Fig. 7), under a newly formed, ragged, yet rapidly rotating wall cloud. As we repositioned to avoid both the south-southeastward-moving tornado and nearby giant hail being reported to its east, the tornado developed a full condensation funnel and became rain-wrapped while still visible (Fig. 8), dissipating about 3 min after genesis. In the process, it damaged a trailer's roof, attaining an EF1 rating on the enhanced Fujita scale (WSEC 2006; Doswell et al. 2009; Edwards et al. 2013) from a later survey by Norman NWS staff, with stated path-length of 1 mi (1.6 km).

Barth et al. (2015) briefly noted the subsequent merger of the LM and RM storms, but without mentioning the LM outflow boundary and its apparent role in prior RM tornadogenesis. During the 0127–0150 UTC interval, the LM cell expanded northwestward along its rear flank, within the RM inflow region, and took a cyclonically curving net turn into the RM storm's own expanding forward flank (Fig. 2 and in the online supplemental animation). The net result was a brief Fujiwhara (1921) type pivot of the two rotating storms' centroids as they merged, followed by wholesale disorganization into a large, weakening multicellular cluster. Meanwhile, around 0117 UTC, a new thunderstorm developed in western Canadian County near Interstate 40, on or just behind the LM gust front, ahead of the RM outflow boundary, and east of the dryline. This convection evolved into an ultimately nontornadic RM supercell by 0142 UTC. It became the first and leading member of a northwest–southeast-aligned chain of three RM supercells that developed along the extrapolated track of the LM gust front (overshot by lowest beam elevations), within a 30-min period. Having escaped southward from the messy and potentially hazardous RM/LM storm merger, we observed the newer, LM-boundary-initiated RM supercell in twilight from near Bridge Creek, Oklahoma (Fig. 9), for about 30 min, as it moved southeastward to the south and southeast of El Reno, then weakened atop both its own outflow and residual boundary layer LM effluent. The next day, DC3 flights identified upper-tropospheric chemical signatures of the tornadic RM storm over the southern Appalachians (Barth et al. 2015).

3. Conclusions and discussion

Heightened local tornado potential, accompanying the ingestion of cyclonically curved outflow by an RM mesocyclone, was recognized afield in this case, as well as at SPC, each as a somewhat speculative "educated guess" based on schematic conceptualization. Today, such short-fused tornado threat similarly may be anticipated in the operational setting, reinforced by understanding from research published before and since. Simulations of storm mergers involving RM supercells (e.g., Hastings

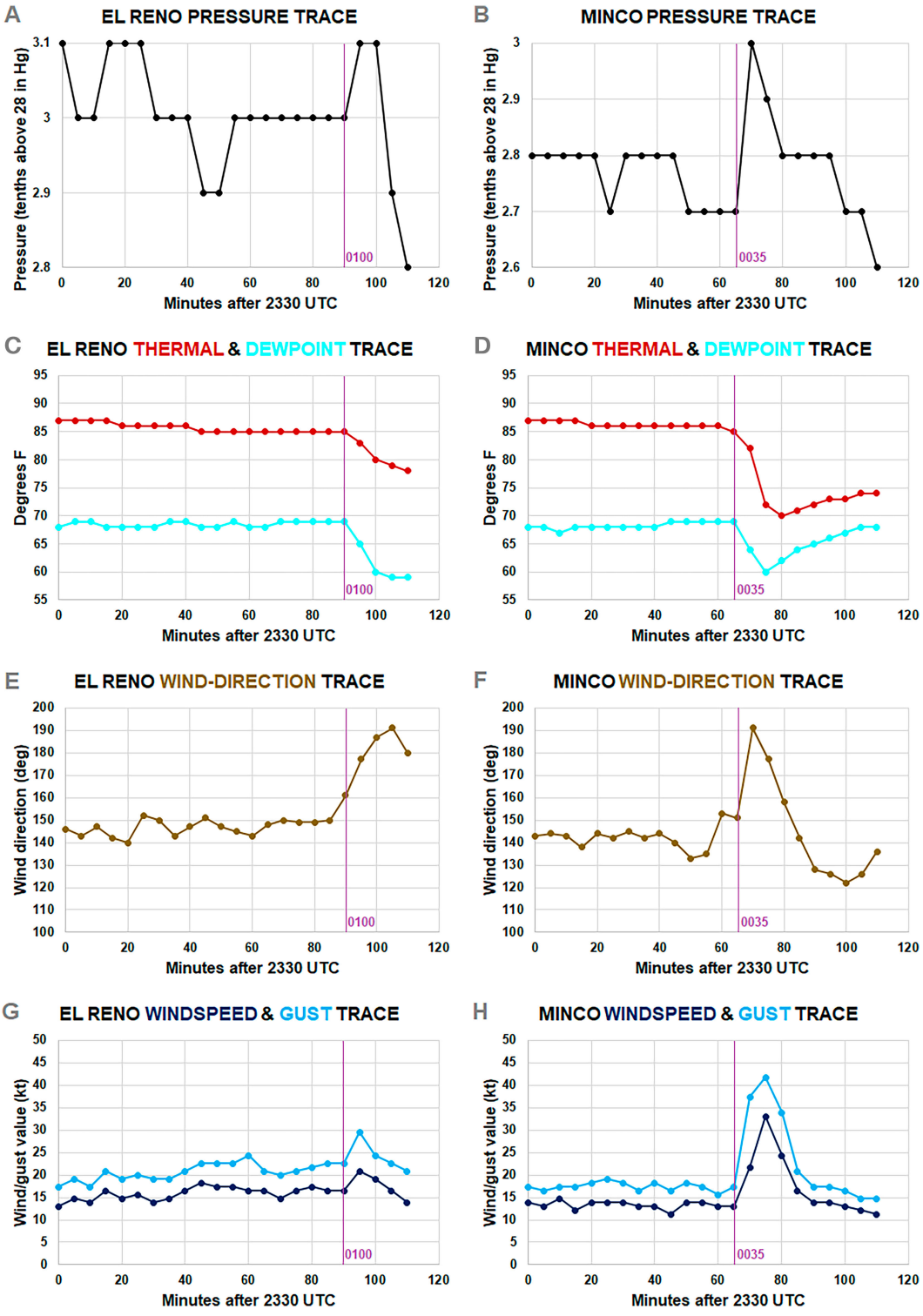

FIG. 6. For (left) El Reno and (right) Minco Oklahoma Mesonet stations, respectively, at identical 5-min intervals beginning at 2330 UTC 29 May 2012, traces of (a),(b) pressure; (c),(d) temperature (brick red) and dewpoint (cyan); (e),(f) wind direction (brown); and (g),(h) 3-s wind speed (dark blue) with gust (light blue). Units as labeled. LM gust-front passage time denoted by purple line with label (UTC). Ordinates are scaled consistently from right to left except for pressure in (a) and (b).

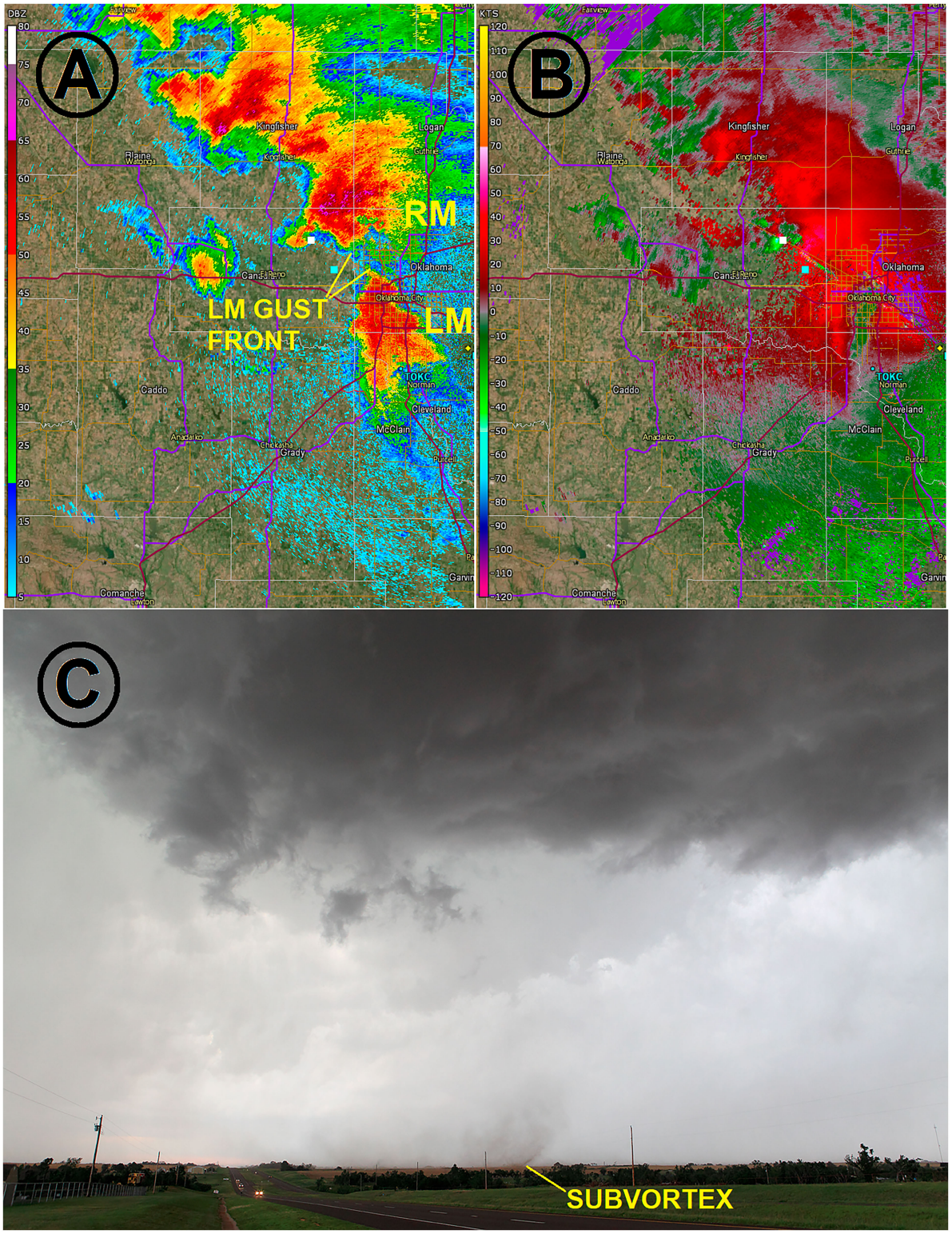

FIG. 7. (a)–(c) As in Fig. 4, but for visible tornadogenesis at 0121 UTC photo time, shot from 35.6383°, −97.8234° at 24-mm focal length, looking northwest. The radar product time was 1 min later. The cyan square represents the approximate location of the Fig. 8 photo. In (c), note the tornadic, concave dust plume beneath a ragged wall cloud (which was rotating strongly). A small, outward-tilted subvortex (labeled) is evident in the northeast (right) rim of the dust plume, and was rotating cyclonically. Dense precipitation is evident at left, southwest of the tornado, manifesting a cascade to surface of the hook-echo reflectivity shown in (a).

FIG. 8. Rain-wrapped tornado (seen at lower center) with fullest funnel condensation, looking northwest from between Piedmont and Yukon, OK, at ≈0125 UTC. A nontornadic wall cloud appears southeast (in front) of the tornado. (Photo by William T. Reid, used by permission.)

and Richardson 2016) have indicated that both strength and separation distance of the merging storm's outflow from the RM updraft influence the latter's survival and mode. In this case, the observed process represents a mixture of results from their simulations: the periphery of LM outflow appeared to benefit RM strength and tornado potential on a time scale of minutes, though the LM outflow's intensity, proximity and large size ultimately led to full merger and mutual demise of both storms.

Observed cell mergers along RM paths are common (e.g., Flournoy et al. 2022; Lyza and Flournoy 2023); however, the former's climatology includes numerous nonsupercellular mergers into RMs. They found RM mesocyclone behavior following merger to be highly variable, and roughly even between strengthening and weakening. Both studies suggested that mergers were more likely to lead to intensification of weak RM mesocyclones and vice versa; however:

1) Our case featured tornadogenesis prior to merger, but immediately after LM gust-front ingestion; and
2) Fischer et al. (2023), commenting on Flournoy et al. (2022) and Lyza and Flournoy (2023), analyzed large-sample, radar-based supercell datasets with null cases, finding that the seemingly inverse intensity tendencies described in the prior papers were stochastic, not necessarily merger-related.

Nondestructive cell mergers into RM supercells have been well-documented (e.g., Lee et al. 2006; Tanamachi et al. 2015—both involving tornadic RMs also witnessed and photographed by the lead author). Those, however, were not in the form of large, mature, long-lived LM supercells acting as RM impactors. Post-LM–RM merger tornado production from an already tornadic RM storm also has been studied (e.g., Lindsey and Bunkers 2005). In their case, a however, each of two RMs in the tristate region of Oklahoma, Missouri and Kansas already had been tornadic, were penetrated by an LM supercell between tornado cycles, and after a pause probably caused by ingestion of relatively stable LM outflow, survived to produce long-track tornadoes. In our event, the merger ultimately destroyed both storms. Figure 6d reveals a substantially stronger LM thermal deficit, compared to the ≈1°–2°C Oklahoma Mesonet-measured drop in Lindsey and Bunkers (2005) for the southern of their two LMs. In that context, the 29 May 2012 storms' mutual demise is unsurprising. Unlike in those cases, ours had LM outflow from the south able to influence a previously nontornadic RM's tornadogenesis, before merger of the supercells' reflectivity cores.

Such a notion, however, is not novel in theory. Fischer and Dahl (2023) documented and modeled four types of supercell interactions: "(i) a chain of two or more supercells, with the southern cell "pumping" outflow into the northern tornadic cell, (ii) a quasi-linear convective system (QLCS) or outflow boundary impacting a supercell from the west, (iii) a previously discrete storm merging with the supercell either before or during tornadogenesis (in many cases these were relatively small cells merging in the supercell inflow region), and (iv) convection along the flanking line of the supercell, with the flanking-line storms producing outflow that influenced the supercell." Though our case has at least minor elements of all four processes, it most strongly conforms to their first archetype, but with a southern (LM in this case) outflow appearing to influence tornadogenesis directly.

Based on observed events such as ours, as well as the Fischer and Dahl (2023) work and accompanying references, situational

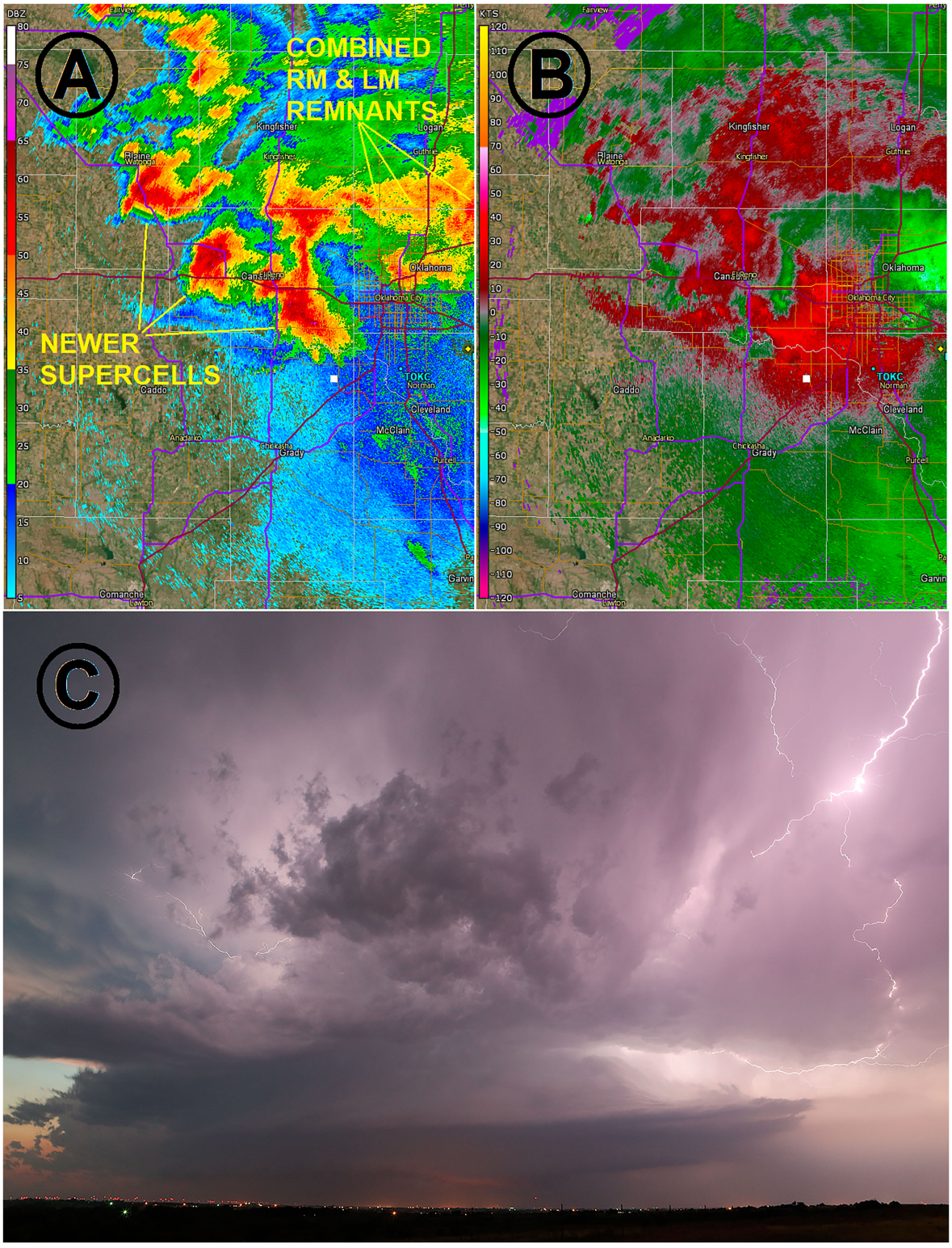

FIG. 9. As in Fig. 7, but for 0222 UTC (radar and photo time) of separate, twilight RM supercells. Weakening multicell remnants of the original RM and LM supercells' merger are labeled. Photo looking northwest from 35.2476°, −97.7343° toward the southeasternmost of the newer supercells labeled.

awareness and understanding of similar supercell/boundary interactions may be useful operationally to identify locally enhanced tornado potential in the spatiotemporal watch–warning gap. This is consistent with the NOAA Forecasting a Continuum of Environmental Threats (FACETs) concept (Rothfusz et al. 2018), involving continuous provision of weather-hazard guidance to end users between what now are convective watch (~6 h) and warning (~15-min) time frames. In the meantime—pre-FACETS implementation—careful diagnosis of potentially favorable storm/boundary interactions may be ascertained operationally in time to issue short meso-γ-scale discussions at SPC, and/or special or severe weather statements (as appropriate) at the local forecast office, addressing a forthcoming brief increase in localized tornado potential near an RM supercell's anticipated mesocyclone track. In keeping with the three case-study criteria of Schultz (2010), we offer this work as a demonstration of an uncommon event with a blend of observations (data and visual), tied to recent theoretical application.

Acknowledgments. Andrew Lyons (SPC) prepared the radar loops in the supplemental material. Israel Jirak of SPC performed astute internal review. The SPC Science Support Branch provided and maintained analytic hardware and software used to perform this study. Conrad Ziegler of NSSL and his DC3 crew shared insightful real-time data with us on the event day. Dr. Ziegler also provided additional project information and insights specifically for this manuscript, along with the mobile-mesonet data. The field observing was self-funded on our own time. We thank the formal reviewers for their time and effort in helping to improve the manuscript. Ideas expressed here are those of the authors, and do not necessarily reflect the views of NWS, NOAA, or the Department of Commerce.

Data availability statement. Radar data came from the Amazon Web Services' public-domain WSR-88D single-site archive (https://s3.amazonaws.com/noaa-nexrad-level2/index.html). Storm reports are available via digitized NCEI *Storm Data* (https://www.ncdc.noaa.gov/stormevents/). Oklahoma Mesonet (https://mesonet.org/) supplied 5-min raw surface data for four sites crossed by the LM gust front. A spreadsheet of the case-specific data also is available from the lead author, as are DC3-supplied MM data used in our analysis. For noncommercial/nonprofit educational and scientific use, photographs may be obtained at no cost from the lead author.

REFERENCES

Barth, M. C., and Coauthors, 2015: The Deep Convective Clouds and Chemistry (DC3) field campaign. *Bull. Amer. Meteor. Soc.*, **96**, 1281–1309, https://doi.org/10.1175/BAMS-D-13-00290.1.

Beatty, K., E. N. Rasmussen, and J. M. Straka, 2008: The supercell spectrum. Part I: A review of research related to supercell precipitation morphology. *Electron. J. Severe Storms Meteor.*, **3** (4), https://doi.org/10.55599/ejssm.v3i4.17.

Beck, J., and C. Weiss, 2013: An assessment of low-level baroclinity and vorticity within a simulated supercell. *Mon. Wea. Rev.*, **141**, 649–669, https://doi.org/10.1175/MWR-D-11-00115.1.

Blair, S. F., D. R. Deroche, J. M. Boustead, J. W. Leighton, B. L. Barjenbruch, and W. P. Gargan, 2011: A radar-based assessment of the detectability of giant hail. *Electron. J. Severe Storms Meteor.*, **6** (7), https://doi.org/10.55599/ejssm.v6i7.34.

Blumberg, W. G., K. T. Halbert, T. A. Supinie, P. T. Marsh, R. L. Thompson, and J. A. Hart, 2017: SHARPpy: An open-source sounding analysis toolkit for the atmospheric sciences. *Bull. Amer. Meteor. Soc.*, **98**, 1625–1636, https://doi.org/10.1175/BAMS-D-15-00309.1.

Brock, F. V., K. C. Crawford, R. L. Elliott, G. W. Cuperus, S. J. Stadler, H. L. Johnson, and M. D. Eilts, 1995: The Oklahoma Mesonet: A technical overview. *J. Atmos. Oceanic Technol.*, **12**, 5–19, https://doi.org/10.1175/1520-0426(1995)012<0005:TOMATO>2.0.CO;2.

Bunkers, M. J., B. A. Klimowski, J. W. Zeitler, R. L. Thompson, and M. L. Weisman, 2000: Predicting supercell motion using a new hodograph technique. *Wea. Forecasting*, **15**, 61–79, https://doi.org/10.1175/1520-0434(2000)015<0061:PSMUAN>2.0.CO;2.

——, D. A. Barber, R. L. Thompson, R. Edwards, and J. M. Garner, 2014: Choosing a universal mean wind for supercell motion prediction. *J. Oper. Meteor.*, **2**, 115–129, https://doi.org/10.15191/nwajom.2014.0211.

Davenport, C. E., C. L. Ziegler, and M. I. Biggerstaff, 2019: Creating a more realistic idealized supercell thunderstorm evolution via incorporation of base-state environmental variability. *Mon. Wea. Rev.*, **147**, 4177–4198, https://doi.org/10.1175/MWR-D-18-0447.1.

Doswell, C. A., III, 1985: The operational meteorology of convective weather. Volume II: Storm scale analysis. NOAA Tech. Memo. ERL ES6-15, 250 pp., https://repository.library.noaa.gov/view/noaa/11215.

——, H. E. Brooks, and N. Dotzek, 2009: On the implementation of the enhanced Fujita scale in the USA. *Atmos. Res.*, **93**, 554–563, https://doi.org/10.1016/j.atmosres.2008.11.003.

Edwards, R., and S. J. Hodanish, 2006: Photographic documentation and environmental analysis of an intense, anticyclonic supercell on the Colorado Plains. *Mon. Wea. Rev.*, **134**, 3753–3763, https://doi.org/10.1175/MWR3296.1.

——, R. L. Thompson, and J. G. LaDue, 2000: Initiation of Storm A (3 May 1999) along a possible horizontal convective roll. Preprints, *20th Conf. on Severe Local Storms*, Orlando, FL, Amer. Meteor. Soc., P1.1, https://ams.confex.com/ams/Sept2000/webprogram/Paper16310.html.

——, J. G. LaDue, J. T. Ferree, K. Scharfenberg, C. Maier, and W. L. Coulbourne, 2013: Tornado intensity estimation: Past, present, and future. *Bull. Amer. Meteor. Soc.*, **94**, 641–653, https://doi.org/10.1175/BAMS-D-11-00006.1.

——, G. W. Carbin, and S. F. Corfidi, 2015: Overview of the Storm Prediction Center. *Proc. 13th History Symp.*, Phoenix, AZ, Amer. Meteor. Soc., 1.1, https://ams.confex.com/ams/95Annual/webprogram/Paper266329.html.

Fischer, J., and J. M. L. Dahl, 2023: Supercell-external storms and boundaries acting as catalysts for tornadogenesis. *Mon. Wea. Rev.*, **151**, 23–38, https://doi.org/10.1175/MWR-D-22-0026.1.

——, M. D. Flournoy, and A. W. Lyza, 2023: Comments on "A climatology of cell mergers with supercells and their association with mesocyclone evolution" and "The influence of cell mergers on supercell characteristics and tornado evolution on 27–28 April 2011." *Mon. Wea. Rev.*, **151**, 2541–2545, https://doi.org/10.1175/MWR-D-23-0120.1.

Flournoy, M. D., A. W. Lyza, M. A. Satrio, M. R. Diedrichsen, M. C. Coniglio, and S. Waugh, 2022: A climatology of cell mergers with supercells and their association with mesocyclone

evolution. *Mon. Wea. Rev.*, **150**, 451–461, https://doi.org/10.1175/MWR-D-21-0204.1.

Fujiwhara, S., 1921: The natural tendency towards symmetry of motion and its application as a principle in meteorology. *Quart. J. Roy. Meteor. Soc.*, **47**, 287–292, https://doi.org/10.1002/qj.49704720010.

Hastings, R., and Y. Richardson, 2016: Long-term morphological changes in simulated supercells following mergers with nascent supercells in directionally varying shear. *Mon. Wea. Rev.*, **144**, 471–499, https://doi.org/10.1175/MWR-D-15-0193.1.

Lee, B. D., B. F. Jewett, and R. B. Wilhelmson, 2006: The 19 April 1996 Illinois tornado outbreak. Part II: Cell mergers and associated tornado incidence. *Wea. Forecasting*, **21**, 449–464, https://doi.org/10.1175/WAF943.1.

Lemon, L. R., and C. A. Doswell III, 1979: Severe thunderstorm evolution and mesocyclone structure as related to tornadogenesis. *Mon. Wea. Rev.*, **107**, 1184–1197, https://doi.org/10.1175/1520-0493(1979)107<1184:STEAMS>2.0.CO;2.

Lindsey, D. T., and M. J. Bunkers, 2005: Observations of a severe, left-moving supercell on 4 May 2003. *Wea. Forecasting*, **20**, 15–22, https://doi.org/10.1175/WAF-830.1.

Lyza, A. W., and M. D. Flournoy, 2023: The influence of cell mergers on supercell characteristics and tornado evolution on 27–28 April 2011. *Mon. Wea. Rev.*, **151**, 1551–1569, https://doi.org/10.1175/MWR-D-22-0189.1.

Markowski, P. M., E. N. Rasmussen, and J. M. Straka, 1998: The occurrence of tornadoes in supercells interacting with boundaries during VORTEX-95. *Wea. Forecasting*, **13**, 852–859, https://doi.org/10.1175/1520-0434(1998)013<0852:TOOTIS>2.0.CO;2.

Potvin, C. K., K. L. Elmore, and S. J. Weiss, 2010: Assessing the impacts of proximity sounding criteria on the climatology of significant tornado environments. *Wea. Forecasting*, **25**, 921–930, https://doi.org/10.1175/2010WAF2222368.1.

Rothfusz, L. P., R. Schneider, D. Novak, K. Klockow-McClain, A. E. Gerard, C. Karstens, G. J. Stumpf, and T. M. Smith, 2018: FACETs: A proposed next-generation paradigm for high-impact weather forecasting. *Bull. Amer. Meteor. Soc.*, **99**, 2025–2043, https://doi.org/10.1175/BAMS-D-16-0100.1.

Schaefer, J. T., and R. Edwards, 1999: The SPC tornado/severe thunderstorm database. Preprints, *11th Conf. on Applied Climatology*, Dallas, TX, Amer. Meteor. Soc., 6.11, https://ams.confex.com/ams/older/99annual/abstracts/1360.htm.

Schultz, D. M., 2010: How to research and write effective case studies in meteorology. *Electron. J. Severe Storms Meteor.*, **5** (2), https://doi.org/10.55599/ejssm.v5i2.22.

Smith, B. T., R. L. Thompson, J. S. Grams, C. Broyles, and H. E. Brooks, 2012: Convective modes for significant severe thunderstorms in the contiguous United States. Part I: Storm classification and climatology. *Wea. Forecasting*, **27**, 1114–1135, https://doi.org/10.1175/WAF-D-11-00115.1.

Tanamachi, R. L., P. L. Heinselman, and L. J. Wicker, 2015: Impacts of a storm merger on the 24 May 2011 El Reno, Oklahoma, tornadic supercell. *Wea. Forecasting*, **30**, 501–524, https://doi.org/10.1175/WAF-D-14-00164.1.

Thompson, R. L., and R. Edwards, 2000: An overview of environmental conditions and forecast implications of the 3 May 1999 tornado outbreak. *Wea. Forecasting*, **15**, 682–699, https://doi.org/10.1175/1520-0434(2000)015<0682:AOOECA>2.0.CO;2.

——, B. T. Smith, J. S. Grams, A. R. Dean, and C. Broyles, 2012: Convective modes for significant severe thunderstorms in the contiguous United States. Part II: Supercell and QLCS tornado environments. *Wea. Forecasting*, **27**, 1136–1154, https://doi.org/10.1175/WAF-D-11-00116.1.

Waugh, S. M., C. L. Ziegler, D. R. MacGorman, S. E. Fredrickson, D. W. Kennedy, and W. D. Rust, 2015: A balloonborne particle size, imaging, and velocity probe for in situ microphysical measurements. *J. Atmos. Oceanic Technol.*, **32**, 1562–1580, https://doi.org/10.1175/JTECH-D-14-00216.1.

Weckwerth, T. M., J. W. Wilson, R. M. Wakimoto, and N. A. Cook, 1997: Horizontal convective rolls: Determining the environmental conditions supporting their existence and characteristics. *Mon. Wea. Rev.*, **125**, 505–526, https://doi.org/10.1175/1520-0493(1997)125<0505:HCRDTE>2.0.CO;2.

Wilson, J. W., T. M. Weckwerth, J. Vivekanandan, R. M. Wakimoto, and R. W. Russell, 1994: Boundary layer clear-air radar echoes: Origin of echoes and accuracy of derived winds. *J. Atmos. Oceanic Technol.*, **11**, 1184–1206, https://doi.org/10.1175/1520-0426(1994)011<1184:BLCARE>2.0.CO;2.

WSEC, 2006: A recommendation for an Enhanced Fujita scale (EF-scale), revision 2. Wind Science and Engineering Center Rep., Texas Tech University, 111 pp., https://www.spc.noaa.gov/efscale/ef-ttu.pdf.